

Inverse scattering of 2d photonic structures by layer-stripping

Marte P. Hatlo Andresen,¹ Harald E. Krogstad¹, and Johannes Skaar^{2,3,*}

¹*Department of Mathematical Sciences, Norwegian University of Science and Technology,
NO-7491 Trondheim, Norway*

²*Department of Electronics and Telecommunications, Norwegian University of Science and
Technology,
NO-7491 Trondheim, Norway*

³*University Graduate Center,
NO-2027 Kjeller, Norway*

**Corresponding author: johannes.skaar@iet.ntnu.no*

Design and reconstruction of 2d and 3d photonic structures are usually carried out by forward simulations combined with optimization or intuition. Reconstruction by means of layer-stripping has been applied in seismic processing as well as in design and characterization of 1d photonic structures such as fiber Bragg gratings. Layer-stripping is based on causality, where the earliest scattered light is used to recover the structure layer-by-layer.

Our set-up is a 2d layered nonmagnetic structure probed by plane polarized harmonic waves entering normal to the layers. It is assumed that the dielectric permittivity in each layer only varies orthogonal to the polarization. Based on obtained reflectance data covering a suitable frequency interval, time-localized pulse data are synthesized and applied to reconstruct the refractive index profile in the leftmost layer by identifying the local, time-domain Fresnel reflection at each point. Once the first layer is known, its impact on the reflectance data is stripped off, and the procedure repeated for the next layer.

Through numerical simulations it will be demonstrated that it is possible to reconstruct structures consisting of several layers. The impact of evanescent modes and limited bandwidth is discussed.

© 2013 Optical Society of America

OCIS codes: 050.5298, 290.3200.

I. Introduction

Photonic crystals have been an exciting field of research since Eli Yablonovitch and Sajeev John published their papers in 1987 [1,2]. Photonic crystals are periodic structures designed to affect the propagation of electromagnetic waves [3]. The usual way of constructing such optical components is to carry out numerical simulations of electromagnetic waves hitting and being scattered off a trial design. The design is then changed by optimization or intuition until the structure has the desired properties. In this paper we use a layer-stripping procedure to show that it is possible to reconstruct a photonic structure from a set of reflectance data based on harmonic waves. In other words, we will look at how the inverse problem can be solved. The ultimate goal is to be able to reconstruct the structures from the observations and use this as a supplementary tool for the design of structures with desired features.

The idea of layer-stripping is to reconstruct the properties of a medium from scattered data originating from an emitted wave pulse on the boundary of the domain. Layer-stripping is based on causality, where the earliest scattered wave from each depth layer is used to recover the structure layer-by-layer. The method was first used in solving inverse acoustic scattering problems for seismic data; overviews can be found in [4,5]. Later, the method has also been applied to the design and characterization of one-dimensional photonic crystal structures such as fiber Bragg gratings [6] and multimode structures [7].

In the present simulation study, we are considering a two-dimensional structure, layered normal to the z -direction, with periodically varying refractive index in the x -direction while being constant in the y -direction. The structure is probed by plane polarized harmonic electromagnetic waves traveling in the z -direction, with the electric field vector pointing in the y -direction, thus representing a two-dimensional wave propagation problem.

The forward problem, consisting of obtaining reflectance data for a known structure, may be formulated in terms of transfer matrices, providing reflection and transmission matrices for each layer as well as the whole structure. The corresponding inverse problem, consisting of recovering the properties of the unknown structure from the reflectance data, requires data for several wave numbers and a range of frequencies.

The key step of the synthetic layer-stripping algorithm is to combine reflectance data for different frequencies so as to synthesize data from a short pulse at the time the pulse hits the surface. The data may then be applied to reconstruct the refractive index profile in the leftmost layer by identifying the local, time-domain Fresnel reflection at each point. Once the first layer is known, its transfer matrix may be computed, and the impact of the layer on the reflectance data eliminated. The same idea is then applied to the modified reflectance data, and continuing in the same way we are, at least in principle, able to reconstruct the whole structure.

II. The forward problem

We are considering photonic crystals consisting of homogeneous, dielectric and nonmagnetic ($\mu = \mu_0$) materials, where the dielectric permittivity, $\epsilon(x, z)$, is varying in the x - and z -directions, and being constant in the y -direction. The structure consists of layers orthogonal to the z -axis, with ϵ constant with respect to z (and y) in each layer. We assume that the structure contains N layers of finite thickness occupying the space from $z_0 = 0$ to z_N . Layer i spans $z_{i-1} \leq z \leq z_i$, with a thickness $\Delta_i = z_i - z_{i-1}$, and permittivity $\epsilon_i(x)$. Outside the structure we assume that it is vacuum. By inserting the Fourier transform in time of the electric and magnetic fields, e.g.

$$\mathbf{E}(\mathbf{x}, t) = \frac{1}{2\pi} \int_{-\infty}^{\infty} \mathbf{e}(x, z, \omega) e^{-i\omega t} d\omega, \quad (1)$$

and similarly for \mathbf{H} , into Maxwell's equations, we obtain

$$\nabla \times \mathbf{e}(x, z, \omega) - i\omega\mu_0 \mathbf{h}(x, z, \omega) = 0, \quad (2)$$

$$\nabla \times \mathbf{h}(x, z, \omega) + i\omega\epsilon_0 \epsilon(x, z) \mathbf{e}(x, z, \omega) = 0, \quad (3)$$

$$\nabla \cdot (\epsilon(x, z) \mathbf{e}(x, z, \omega)) = 0, \quad (4)$$

$$\nabla \cdot \mathbf{h}(x, z, \omega) = 0. \quad (5)$$

In addition, from the standard continuity conditions for \mathbf{E} and \mathbf{H} , parallel (\parallel) and orthogonal (\perp) to the layer boundaries, the following conditions have to apply

$$\epsilon_1 \mathbf{e}_1^\perp = \epsilon_2 \mathbf{e}_2^\perp, \quad (6)$$

$$\mathbf{e}_1^\parallel = \mathbf{e}_2^\parallel, \quad (7)$$

$$\mathbf{h}_1 = \mathbf{h}_2. \quad (8)$$

Omitting the dependence of ω , direct substitution shows that the Fourier transformed Maxwell's equations in the present case admit solutions of the form

$$\mathbf{e}(x, z) = e(x, z) \hat{\mathbf{y}}, \quad (9)$$

$$\mathbf{h}(x, z) = \frac{1}{i\omega\mu_0} \left(-\frac{\partial e(x, z)}{\partial z} \hat{\mathbf{x}} + \frac{\partial e(x, z)}{\partial x} \hat{\mathbf{z}} \right), \quad (10)$$

provided $e(x, z)$ satisfies the scalar Helmholtz equation,

$$\frac{\partial^2 e}{\partial x^2} + \frac{\partial^2 e}{\partial z^2} + \epsilon(x, z) k^2 e = 0, \quad (11)$$

where $k = \omega/c_0$, $c_0^2 = 1/\mu_0\epsilon_0$, and e as well as its partial derivatives are continuous across the layer boundaries.

The structure will be probed using the plane polarized waves in Eqs. (9) and (10), and all transmitted and reflected waves will have the same polarization.

The direct problem consists of solving Eq. (11) with appropriate boundary conditions. These will be plane waves entering from the half space $z \leq 0$ (thus, having positive z -component wave numbers), whereas no waves are supposed to enter the structure from the region $z > z_N$.

III. Solution by transfer matrices

Let L be the extension of the computational domain in the x -direction. By imposing L -periodic boundary conditions, we may expand the electric field and the permittivity into the Fourier series

$$\mathbf{e}(x, z) = e(x, z)\hat{\mathbf{y}} = \sum_m E^{(m)}(z) \exp(ik_x^{(m)}x)\hat{\mathbf{y}}, \quad (12)$$

$$\epsilon(x, z) = \sum_m \epsilon^{(m)}(z) \exp(ik_x^{(m)}x), \quad (13)$$

where $k_x^{(m)} = 2\pi m/L$. The Fourier components are given as

$$\epsilon^{(m)}(z) = \frac{1}{L} \int_0^L \epsilon(x, z) \exp(-ik_x^{(m)}x) dx. \quad (14)$$

By inserting the Fourier series into Helmholtz' equation we obtain

$$\frac{d^2 E^{(m)}(z)}{dz^2} - (k_x^{(m)})^2 E^{(m)}(z) + k^2 \sum_{m'} \epsilon^{(m-m')}(z) E^{(m')}(z) = 0, \quad (15)$$

for each m . Let $\mathbf{E} = \{E^{(m)}\}_{m \in \mathbb{Z}}$ and use $k^2 = (k_x^{(m)})^2 + (k_z^{(m)})^2$. We may then write Eq. (15) as the matrix equation

$$\frac{d^2 \mathbf{E}(z)}{dz^2} + (\mathbf{k}_z^2 + \mathbf{V}(z)) \mathbf{E}(z) = 0, \quad (16)$$

where $\mathbf{k}_z = \text{diag}(k_z^{(m)})$, and $\mathbf{V}(z)$ is the infinite dimensional Toeplitz matrix operator defined as

$$\mathbf{V}(z) = -k^2 \mathbf{I} + k^2 \begin{bmatrix} \ddots & \vdots & & & \\ \dots & \epsilon^{(0)} & \epsilon^{(-1)} & \epsilon^{(-2)} & \\ & \epsilon^{(1)} & \epsilon^{(0)} & \epsilon^{(-1)} & \\ & \epsilon^{(2)} & \epsilon^{(1)} & \epsilon^{(0)} & \dots \\ & & & \vdots & \ddots \end{bmatrix}. \quad (17)$$

Eq. (16) may be decomposed into a first order system by writing $\mathbf{E}(z) = \mathbf{E}^+(z) + \mathbf{E}^-(z)$, and require

$$\frac{d\mathbf{E}^+(z)}{dz} = i\mathbf{k}_z\mathbf{E}^+(z) + i(2\mathbf{k}_z)^{-1}\mathbf{V}(z)(\mathbf{E}^+(z) + \mathbf{E}^-(z)), \quad (18a)$$

$$\frac{d\mathbf{E}^-(z)}{dz} = -i\mathbf{k}_z\mathbf{E}^-(z) - i(2\mathbf{k}_z)^{-1}\mathbf{V}(z)(\mathbf{E}^+(z) + \mathbf{E}^-(z)). \quad (18b)$$

Eq. (16) follows easily from Eqs. (18a) and (18b) after summation and differentiation. Note that outside the structure \mathbf{V} equals zero, and the solution to Eq. (18) are forward and backward going waves.

By writing

$$\Psi(z) = \begin{bmatrix} \mathbf{E}^+(z) \\ \mathbf{E}^-(z) \end{bmatrix}, \quad \mathbf{C}(z) = \begin{bmatrix} i\mathbf{k}_z + i(2\mathbf{k}_z)^{-1}\mathbf{V}(z) & i(2\mathbf{k}_z)^{-1}\mathbf{V}(z) \\ -i(2\mathbf{k}_z)^{-1}\mathbf{V}(z) & -i\mathbf{k}_z - i(2\mathbf{k}_z)^{-1}\mathbf{V}(z) \end{bmatrix}, \quad (19)$$

Eq. (18) can be brought into the compact matrix form

$$\frac{d\Psi(z)}{dz} = \mathbf{C}(z)\Psi(z). \quad (20)$$

Since the permittivity is independent of z within a layer, the matrix \mathbf{C} will be constant for each layer. Thus, Eq. (20) can be integrated to

$$\Psi(z_b) = \exp[(z_b - z_a)\mathbf{C}]\Psi(z_a) \quad (21)$$

for z_a and z_b inside the same layer. Let \mathbf{C}_i be the \mathbf{C} -matrix for layer i . By defining

$$\mathbf{M}_i = \exp(\Delta_i \mathbf{C}_i), \quad (22)$$

we obtain

$$\Psi(z_i) = \mathbf{M}_i \Psi(z_{i-1}). \quad (23)$$

Since e and $\partial e/\partial z$ are continuous across the layer boundaries, \mathbf{E}^+ and \mathbf{E}^- also must be continuous here. By successive applications of Eq. (23) we are able to propagate through the structure from z_0 to z_N ,

$$\Psi(z_N) = \prod_{i=N}^0 \mathbf{M}_i \Psi(z_0) = \mathbf{M} \Psi(z_0). \quad (24)$$

The boundary conditions at $z = z_0 = 0$ are contained in

$$\Psi(z_0) = \begin{bmatrix} \mathbf{E}^+(z_0) \\ \mathbf{E}^-(z_0) \end{bmatrix}, \quad (25)$$

where $\mathbf{E}^+(z_0)$ is given by the probing waves, and $\mathbf{E}^-(z_0)$ is unknown. At the other end of the structure,

$$\Psi(z_N) = \begin{bmatrix} \mathbf{E}^+(z_N) \\ 0 \end{bmatrix}, \quad (26)$$

where $\mathbf{E}^+(z_N)$ has to be determined. If we partition the matrix \mathbf{M} according to the definition of Ψ ,

$$\mathbf{M} = \begin{bmatrix} \mathbf{M}_{11} & \mathbf{M}_{12} \\ \mathbf{M}_{21} & \mathbf{M}_{22} \end{bmatrix}, \quad (27)$$

and consider the matrix equation

$$\begin{bmatrix} \mathbf{E}^+(z_N) \\ 0 \end{bmatrix} = \begin{bmatrix} \mathbf{M}_{11} & \mathbf{M}_{12} \\ \mathbf{M}_{21} & \mathbf{M}_{22} \end{bmatrix} \begin{bmatrix} \mathbf{E}^+(z_0) \\ \mathbf{E}^-(z_0) \end{bmatrix}, \quad (28)$$

the formal solution is easily seen to be

$$\mathbf{E}^-(z_0) = \mathbf{R}\mathbf{E}^+(z_0), \quad (29)$$

$$\mathbf{E}^+(z_N) = \mathbf{T}\mathbf{E}^+(z_0), \quad (30)$$

where \mathbf{R} and \mathbf{T} are the so-called *reflection* and *transmission matrices* for the structure,

$$\mathbf{R} = -\mathbf{M}_{22}^{-1}\mathbf{M}_{21}, \quad (31)$$

$$\mathbf{T} = \mathbf{M}_{11} - \mathbf{M}_{12}\mathbf{M}_{22}^{-1}\mathbf{M}_{21}. \quad (32)$$

The reflection and transmission matrices provide $\mathbf{E}^-(z_0)$ and $\mathbf{E}^+(z_N)$ for all possible input $\mathbf{E}^+(z_0)$.

To solve the inverse problem, we need reflectance data for all possible incident wave numbers. Such a set of excitation-response pairs can be described by the following equation

$$\begin{bmatrix} \mathbf{T} \\ \mathbf{0} \end{bmatrix} = \mathbf{M} \begin{bmatrix} \mathbf{I} \\ \mathbf{R} \end{bmatrix}. \quad (33)$$

Here, each column i of \mathbf{I} corresponds to an experiment where the incident field amplitude is 1 for one of the Fourier components and zero for the others. The i th column of \mathbf{R} is the reflection at z_0 , and the i th column of \mathbf{T} is the corresponding transmission at z_N .

IV. The inverse problem

The inverse problem is solved by combining reflectance data for a range of frequencies, $[\omega_1, \omega_2]$, so as to synthesize data from a short pulse at the time the pulse hits the surface. The permittivity of the layer may then be recovered as described below if the pulse width in time, $\mathcal{O}(10(\omega_2 - \omega_1)^{-1})$, is shorter than the round-trip travel time in the layer, $2\Delta_i/c$. In this study we shall, for simplicity, assume that the layer thicknesses, Δ_i , are known. It is, in principle, possible to do the layer-stripping without knowledge of the layer thickness. This will be briefly discussed this in Sec. VI. From the permittivity and the thickness it is now possible to compute the transfer matrix for the layer, and the impact of the layer removed

from the reflection data. Thus, we obtain reflectance data for the same structure, but without the leftmost layer, and may then repeat the steps above until the entire structure has been reconstructed.

IV.A. Computing the permittivity

Let us assume that we have reflectance data from an experiment where the incident wave is a plane wave pulse, $F(t - z/c_0)$, see Fig. 1. The incident wave enters from $z < 0$, and first hits the leftmost layer of the structure. The wave speed in the first layer is $c_1(x)$.

Let us consider a small neighborhood around the point x , and assume that the permittivity in the leftmost layer is varying slowly enough, so that we may take it to be constant and equal to $\epsilon_1(x)$ inside the area we consider. Furthermore, we restrict our calculation to a small time interval so that the reflected and transmitted waves are only affected by the first layer.

At the left side of the boundary, the electric field will be a sum of the incoming and the reflected wave, and at the right side, the field consists of the transmitted wave. Thus, continuity of the transversal electromagnetic fields gives us

$$F(t - \frac{z}{c_0}) + R_1(x)F(t + \frac{z}{c_0}) = T_1(x)F(t - \frac{z}{c_1(x)}), \quad (34)$$

and

$$-\frac{1}{c_0}F'(t - \frac{z}{c_0}) + \frac{R_1(x)}{c_0}F'(t + \frac{z}{c_0}) = -\frac{T_1(x)}{c_1(x)}F'(t - \frac{z}{c_1(x)}), \quad (35)$$

for some reflection coefficient $R_1(x)$. Obviously, the incident wave pulse F needs to be short for Eqs. (34) and (35) to hold. For $z = 0$ and $0 \leq t \ll \Delta_1/c_0$ we thus have from Eqs. (34) and (35)

$$1 + R_1(x) = T_1(x), \quad (36)$$

$$-1 + R_1(x) = -T_1(x)\frac{c_0}{c_1(x)}, \quad (37)$$

leading to the following expression for the permittivity in the leftmost layer:

$$\epsilon_1(x) = \epsilon_0 \left(\frac{1 - R_1(x)}{1 + R_1(x)} \right)^2. \quad (38)$$

Eq. (38) can be interpreted as a local Fresnel equation; it connects the local reflection coefficient $R_1(x)$ and the local permittivity $\epsilon_1(x)$.

IV.B. Layer-stripping

For the layer-stripping we shall assume that the layer thickness is known. Once we have computed $\epsilon_1(x)$, we obtain the transfer matrix \mathbf{M}_1 from Eq. (22). As in Eq. (23), the forward

and backward going waves just before the second layer can be computed as

$$\begin{bmatrix} \mathbf{E}^+(z_1) \\ \mathbf{E}^-(z_1) \end{bmatrix} = \mathbf{M}_1 \begin{bmatrix} \mathbf{E}^+(z_0) \\ \mathbf{E}^-(z_0) \end{bmatrix} = \mathbf{M}_1 \begin{bmatrix} \mathbf{I} \\ \mathbf{R} \end{bmatrix}. \quad (39)$$

Note that here \mathbf{E}^+ and \mathbf{E}^- are matrices as in Eq. (33). Similar to the solution for the full structure, Eqs. (29) and (30), we may define

$$\mathbf{E}^+(z_N) = \tilde{\mathbf{T}}\mathbf{E}^+(z_1), \quad (40)$$

$$\mathbf{E}^-(z_1) = \tilde{\mathbf{R}}\mathbf{E}^+(z_1), \quad (41)$$

and thus the new reflection matrix can be found as

$$\tilde{\mathbf{R}} = \mathbf{E}^-(z_1)\mathbf{E}^+(z_1)^{-1}. \quad (42)$$

V. Algorithm

For the numerical experiments, which we will discuss in Sec. VI, we first solve the forward problem to obtain valid reflectance data $\mathbf{R}(k_x^{(m')}, k_x^{(m)}, \omega)$ for each of N_ω frequencies in the span $[\omega_1, \omega_2]$. Here $k_x^{(m')}$ denote the incident wave numbers, and $k_x^{(m)}$ the reflected wave numbers.

For the inverse problem, the first step is to synthesize a time localized pulse in space and time to be applied in Eq. (38). Only data for incident waves normal to the structure are used in the identification of the layers. We start with a transformation from $k_x^{(m)}$ to x ,

$$r(x, \omega) = \sum_m \mathbf{R}(k_x^{(m')} = 0, k_x^{(m)}, \omega) e^{ik_x^{(m)}x}, \quad (43)$$

where

$$k_x^{(m)} = \frac{2\pi m}{L}, \quad m \in \mathbb{Z}, \quad \text{and} \quad \omega \in [\omega_1, \omega_2]. \quad (44)$$

Ideally, one would now carry out an inverse Fourier transform in order to obtain the reflected field in the space- and time-domains resulting from an incident delta-pulse,

$$R(x, t) = \frac{1}{2\pi} \int_{-\infty}^{\infty} r(x, \omega) e^{-i\omega t} d\omega. \quad (45)$$

However, since we only know $r(x, \omega)$ in the frequency interval $[\omega_1, \omega_2]$, we need to choose a window function $W(\omega)$ with support in that interval. The corresponding pulse in time is denoted $w(t)$, and the experience with some standard window functions are discussed in the next section. The synthetic response will then be

$$R_w(x, t) = \frac{1}{2\pi} \int_{\omega_1}^{\omega_2} r(x, \omega) W(\omega) e^{-i\omega t} d\omega. \quad (46)$$

For $z = 0$ and $0 \leq t \ll \Delta_1$, we see from Eq. (34) that $R_w(x, t) = R_1(x) w(t)$. Hence, for $t = 0$, we may write

$$R_1(x) = \frac{R_w(x, 0)}{w(0)} = \frac{\int_{\omega_1}^{\omega_2} r(x, \omega) W(\omega) d\omega}{\int W(\omega) d\omega}. \quad (47)$$

The permittivity $\epsilon(x)$ is then obtained from Eq. (38). The layer-stripping has been discussed in Sec. IV.B.

The numerical method may now be summarized in a pseudo code, as follows.

Input to the algorithm: Reflection matrices $\mathbf{R}(k_x^{(m')} = 0, k_x^{(m)}, \omega)$, for $\omega \in [\omega_1, \omega_2]$.

- 1 Transform reflection matrices to the space/frequency domain using Eq. (43). Next, determine the reflection coefficient at $t = 0$ using Eqs. (46) - (47). The permittivity now follows from Eq. (38).
- 2 Use $\epsilon(x)$ and Eq. (14) to find the Fourier components. Then the transfer matrix can be computed from Eqs. (17), (19) and (22).
- 3 Knowing the transfer matrix, the forward and backward going waves before the next layer can be computed from Eq. (39).
- 4 Compute the new reflection matrix, using Eq. (42).
- 5 Return to step 1, to compute the permittivity in the next layer, until all layers have been found.

VI. Numerical experiments

For simplicity, we scale ϵ_0 and μ_0 (in free space) to 1, and hence $c_0 = 1$. Now, the dispersion relation in free space reduces to $k = \omega$, and the wavelengths will be $\lambda = 2\pi/\omega$. The length of the synthesized pulse will depend on the frequency interval $[\omega_1, \omega_2]$, and be of order $2\pi(\omega_2 - \omega_1)^{-1}$. One must require that the pulse length is shorter than the round-trip travel time in the first layer, i.e.

$$\frac{2\pi}{\omega_2 - \omega_1} \lesssim \frac{2\Delta_1}{c_1}. \quad (48)$$

Thus, to be able to reconstruct the structure, we need to make sure that the frequency band is wide enough. Through simulations we have seen that for smaller frequency bands, the error fluctuates as the bandwidth grows. However, as soon as the frequency span is wide enough, the calculations are stable.

As mentioned in Sec. V, we use Eq. (33) to compute reflection matrices. To compute the reflection matrix and solve the inverse problem, the number of Fourier components, M , the computational domain, L , and the N_ω frequencies in the interval $[\omega_1, \omega_2]$, must be

chosen. Now, the reflection and transmission matrices will have dimension $M \times M$ and the propagation matrix \mathbf{M} dimension $2M \times 2M$. Note that given the resolution in the x -direction

$$\Delta x = \frac{L}{M}, \quad (49)$$

the maximum Nyquist wave number is given as

$$\max k_x = \frac{\pi M}{L}. \quad (50)$$

Since

$$k_z = \sqrt{k^2 - k_x^2} = \sqrt{\omega^2 - k_x^2}, \quad (51)$$

evanescent modes in vacuum occur when $\max k_x > \omega$.

As we see in Eq. (42), the updated reflection matrix is a product of the backward traveling waves and the inverse of the forward traveling waves. In a homogeneous medium, the forward and backward traveling waves have the z -dependence $\exp(ik_z z)$ and $\exp(-ik_z z)$, respectively. Thus, when we have evanescent modes with $k_z = iK$ for some $K > 0$, we expect a noise amplification factor of the order of $\exp(2K\Delta)$ when one layer is stripped off. Because of this, we restrict our frequency band to avoid a too large K .

Note that if the variations in the x -direction are fast, we will need a finer resolution in x . To obtain this, we must either make M larger, or L smaller, which again implies that the maximum wave number, $\max k_x$, increases. The result is that we need higher frequencies to avoid evanescent modes. Thus, it is convenient to restrict the attention to structures that vary slowly with respect to x . We will, however, in Example 2 see that we are also able to reconstruct a structure with fast variations.

There are three effects that mainly contribute to the limitations in this method. The first one is the effect of evanescent modes, which was discussed above. The second is related to the contrast between the minimum and maximum refractive indices, n_1 and n_2 . As the contrast grow higher, more of the light is reflected by the first layers. This will in turn make the calculations less accurate [8, 9]. The last effect is also related to the bandwidth. As discussed in the beginning of this section, we need the pulse length to be smaller than the layer round-trip travel time, thus imposing a lower limit to the bandwidth. Conversely, if the bandwidth is fixed, the layer thicknesses have to be large enough.

As discussed in Sec. V, it is necessary to shape the reflection data using some window function. Numerical experiments applying three different window functions on the interval $[\omega_1, \omega_2]$ are presented in Sec. VI.A. As expected, the experiments favor smoother windows over the simple rectangular window. Consequently, a Hanning window has been applied for the rest of the computations.

In all simulations we have assumed that we know the layer thickness. It would, at least in principle, be possible to reconstruct the layer thickness. To do this, one need to use a

fictitious layer thickness, Δz , which must be small compared to the expected layer thickness. Then this Δz can be used in the computations, to reconstruct each layer piece by piece.

All the calculations were done using MATLAB on an Intel Core 2 Quad 2.83 GHz computer. For a typical calculation, the runtime was approximately 260 s. About 180 s was used on calculating the forward problem, i.e. the reflection matrices $\mathbf{R}(k_x^{(m')}, k_x^{(m)}, \omega)$, the calculation of the permittivity is neglectable, and the calculation and removal of the leftmost layer took about 80 s.

VI.A. Example 1

In this example we have chosen a structure where the permittivity within the layers is given as

$$\epsilon(x) = \eta \pm \gamma \cos\left(\frac{x}{2}\right), \quad (52)$$

and where the two different layers are obtained by alternating between $+$ and $-$. The layer thickness has been set to $\pi/2$, and the parameters η and γ are chosen so that

$$\min \epsilon = n_1^2 = 1.0, \quad (53)$$

$$\max \epsilon = n_2^2, \quad (54)$$

i.e. n_1 is kept constant, while n_2^2 is varied. For all the experiments presented here, $M = 300$ and $L = 100$, giving a resolution in x of $1/3$ and a maximum k_x of 3π . The choice of frequency band depends on whether we want to include evanescent modes in the computations, how large K we can tolerate, and the layer thickness.

We first consider the choice of frequency window functions, Eq. (46), by testing three different functions, a simple rectangular window, the Hanning window and the Tukey (tapered cosine) window. The comparisons were carried out for two different values of n_2 , $n_2^2 = 1.2$ for the first test, and $n_2^2 = 2.0$ for the second. The real difference in the choice of window functions can only be seen in the reconstruction of the second layer. Therefore, the results, displayed in Fig. 2, are only shown for this layer. The rectangular window gives poor results already for the lowest refractive index, whereas the two other choices give a nice reconstruction. For the higher index, we see that also the Tukey window is beginning to give less accurate results, while for the Hanning window there is almost no visible difference from the exact curve. For the rest of the numerical examples, we have therefore chosen to use the Hanning window.

Let us now turn to the effect of including evanescent modes. In these experiments, the permittivity was first chosen such that $n_1^2 = 1.0$ and $n_2^2 = 1.05$, and secondly we had $n_1^2 = 1.0$ and $n_2^2 = 2.0$. The frequency bandwidth was set constant to 10, but the lower and upper frequencies were changed to include none, or some evanescent modes. Again, the first layer is nicely reconstructed, so we only show results for the second layer in Fig. 3. Including some

evanescent modes improves the results, but if K gets too large, there are fluctuations in the reconstruction. Note that as n_2 gets higher, a larger K is acceptable. This can be explained by the fact that the field now is locally non-evanescent, since a local k_z in the medium would be $k_z = (n^2\omega^2 - k_x^2)^{1/2}$.

Bigger contrasts in the refractive index may be simulated by keeping the lower index constant at $n_1^2 = 1.0$, while the upper index is changed. The results are shown in Fig. 4 and we see that the first layer is well reconstructed for all choices of n_2^2 , while some fluctuations in the second layer are visible when $n_2^2 > 2$.

Finally, we demonstrate that it is possible to reconstruct more than two layers. Fig. 5 shows the error, given as $|\epsilon_{\text{comp}} - \epsilon|$ for each layer in a structure consisting of four layers. The permittivity was chosen between $n_1^2 = 1.0$ and $n_2^2 = 1.05$.

VI.B. Example 2, a square function

In this example we have chosen the permittivity to be a square function with period 2π in each layer. To get two different layers, and a permittivity between n_1 and n_2 , we let

$$\epsilon_1(x) = \begin{cases} n_2^2, & 0 \leq x < \pi \\ n_1^2, & \pi \leq x < 2\pi, \end{cases} \quad (55)$$

$$\epsilon_2(x) = \begin{cases} n_1^2, & 0 \leq x < \pi \\ n_2^2, & \pi \leq x < 2\pi. \end{cases} \quad (56)$$

This example has been chosen to show that we are able to reconstruct a less smooth function. The fact that the permittivity changes fast seems to be in conflict with the discussion in Sec. VI, but as we see from Fig. 6 we actually manage to reconstruct two layers of this structures as well. The reason it work is that we only use the low frequency components of the square. The results can be seen in Fig. 6.

VII. Conclusion

In this paper we have presented a method for reconstructing 2d photonic structures layer-by-layer. In principle, the reconstruction is exact, and we have shown through numerical examples that we are able to reconstruct different structures consisting of several layers.

There are essentially three, fundamental mechanisms that limit the accuracy in practice: The presence of evanescent modes, accumulated reflection, and limited bandwidth. The fact that evanescent modes lead to inaccuracies means that either the probing frequencies must be sufficiently high, or the spatial transversal frequencies of the structure must be sufficiently small. The second limitation is a result of the fact that if the transmission through the structure is too small, little light reaches the back end. Then the back end has little influence

on the reflection data, and cannot be reconstructed accurately. Finally, the bandwidth must be sufficiently large such that the synthetic, incident pulse is shorter than the round-trip time in all layers. Alternatively, for a fixed, available bandwidth, the structure must vary sufficiently slowly in the longitudinal direction z . In the numerical examples, for a center wavelength $1\text{ }\mu\text{m}$ the normalized frequency interval $[9, 19]$ corresponds to the wavelength interval $[0.74, 1.56]\text{ }\mu\text{m}$. The layer thicknesses in the example become $3.5\text{ }\mu\text{m}$. If the available bandwidth is reduced to 100 nm , the layers must be 5–10 times thicker to achieve the same accuracy.

References

1. E. Yablonovitch, “Inhibited Spontaneous Emission in Solid-State Physics and Electronics”, Phys. Rev. Lett. **58**, 2059-2062 (1987).
2. S. John, “Strong Localization of Photons in Certain Disordered Dielectric Superlattices”, Phys. Rev. Lett. **58**, 2486-2489 (1987).
3. J. D. Joannopoulos, R. D. Meade and J. N. Winn, *Photonic Crystals: Molding the Flow of Light* (Princeton University Press, 1995)
4. A. M. Bruckstein, B. C. Levy and T. Kailath, “Differential Methods in Inverse Scattering”, SIAM J. Appl. Math. **45**, 312-335 (1985).
5. A. E. Yagle and B. C. Levy, “Layer-stripping solutions of multidimensional scattering problems”, J. Math. Phys. **27**, 1701-1710 (1986).
6. J. Skaar, L. Wang and T. Erdogan, “On the Synthesis of Fiber Bragg Gratings by Layer Peeling”, IEEE J. Quantum Electron. **37**, 165-173 (2001).
7. O. H. Waagaard and J. Skaar, “Inverse Scattering in Multimode Structures”, SIAM J. Appl. Math. **68**, 311-333 (2007).
8. A. M. Bruckstein, I. Koltracht, and T. Kailath, “Inverse scattering with noisy data”, SIAM J. Sci. Stat. Comput. **7**, 1331-1349 (1986).
9. J. Skaar and R. Feced, “Reconstruction of gratings from noisy reflection data”, J. Opt. Soc. Am. A **19**, 2229-2237 (2002).

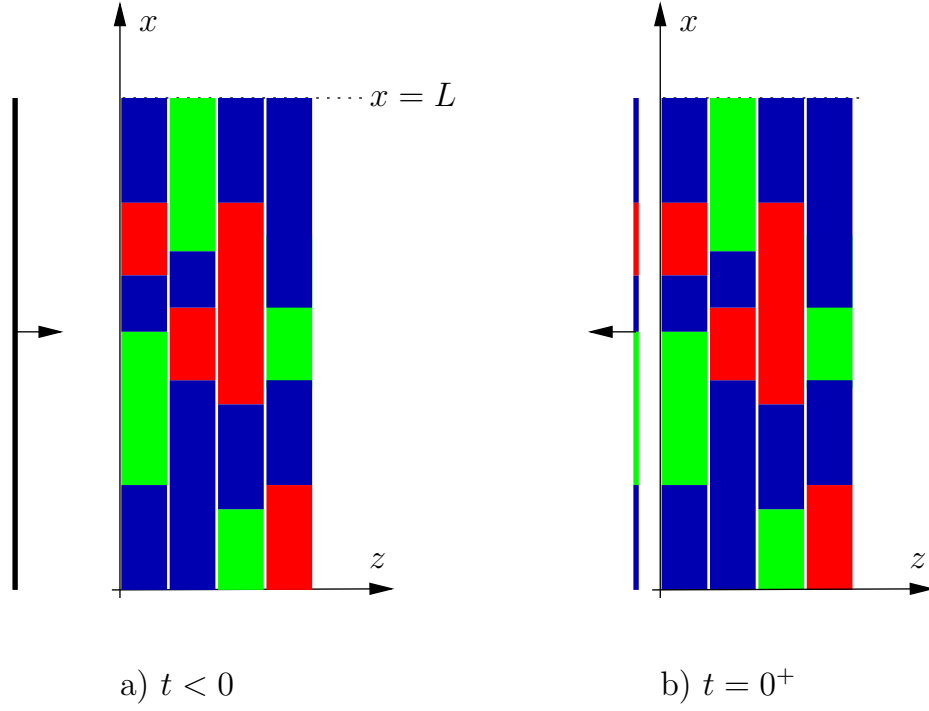


Fig. 1. (a) A plane wave pulse is incident to a layered 2d structure. For the structure different colors indicate different refractive indices. (b) Immediately after $t = 0$ the field has only been affected by the first layer; thus we may identify the first layer from the first part of the reflected field in the time-domain. AKSFig1.eps.

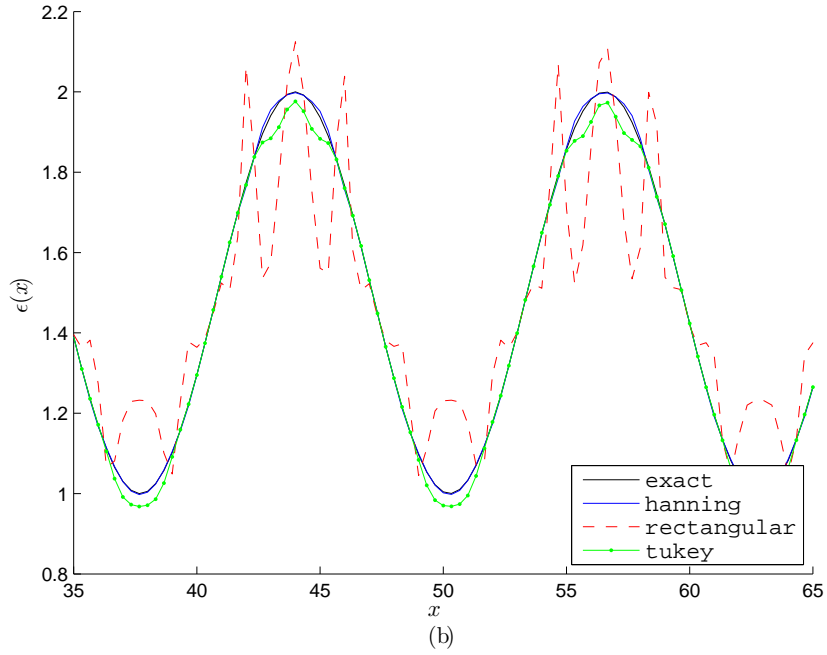
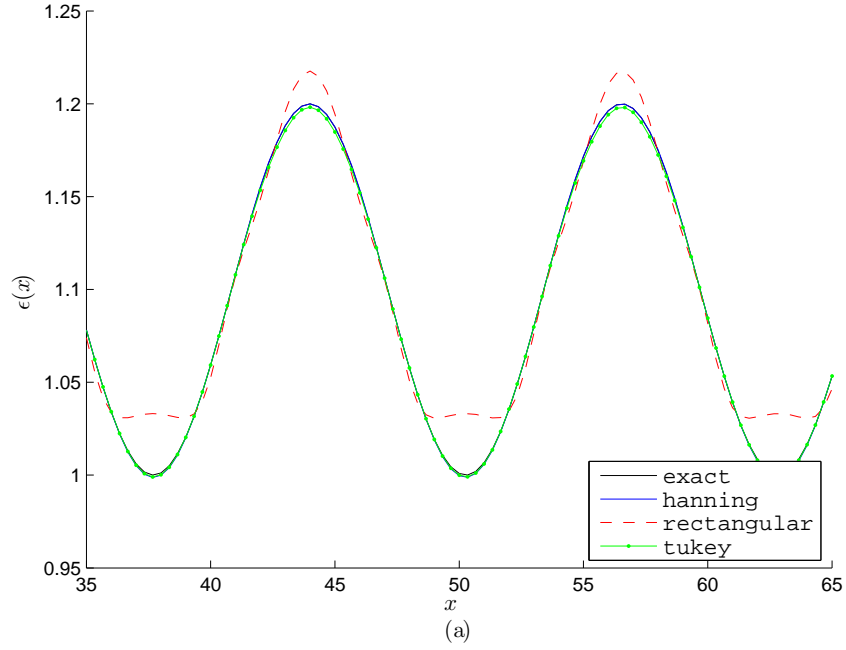


Fig. 2. Reconstruction of the second layer for different window functions, in (a) $n_2^2 = 1.2$ and in (b) $n_2^2 = 2.0$. Other parameters: $M = 300$, $L = 100$, $N_\omega = 100$, $\omega \in [9, 19]$, $\Delta z = \pi/2$, $n_1^2 = 1.0$. Note that only parts of the computational domain L are shown in the plots. AKSFig2.eps.

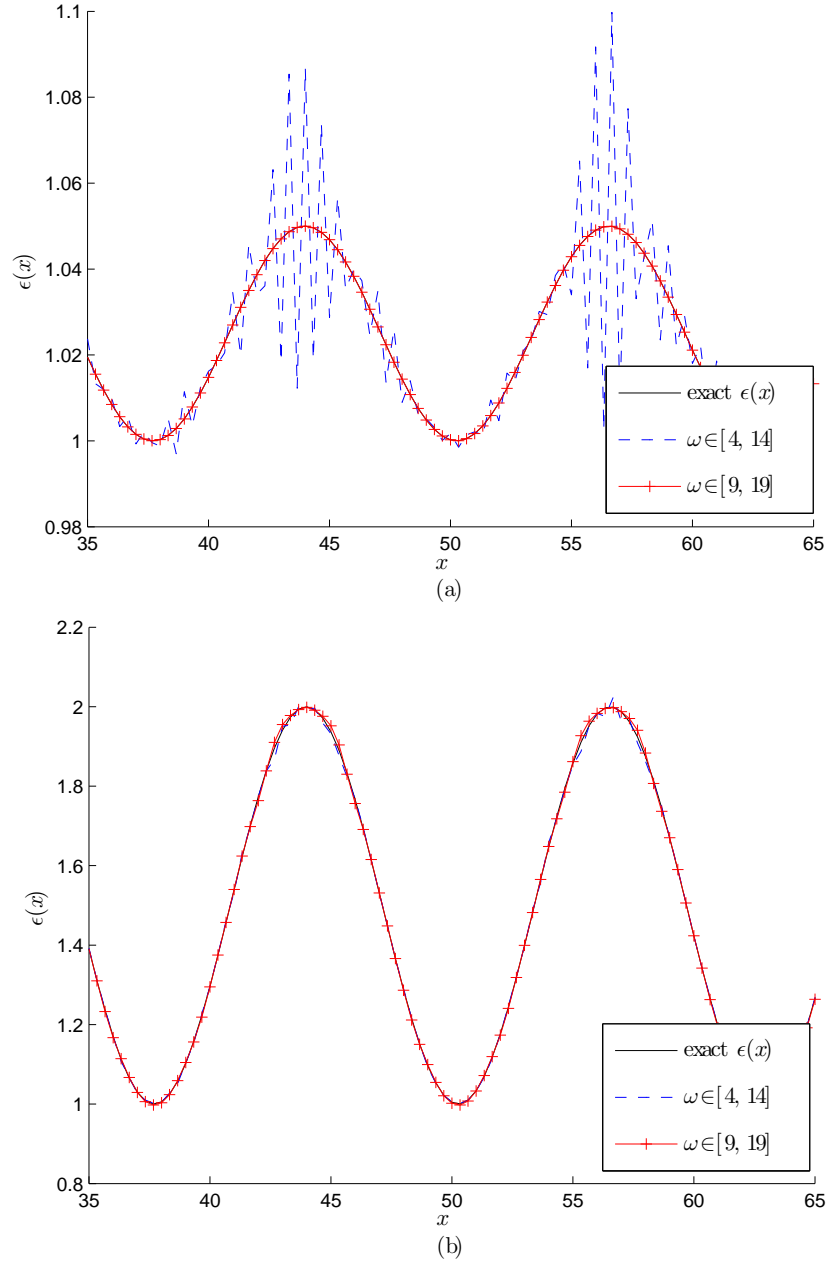


Fig. 3. Reconstruction of the second layer for different ω_1 and ω_2 , but with constant bandwidth. In (a) $n_2^2 = 1.05$, and in (b) $n_2^2 = 2.0$. Other parameters: $M = 300$, $L = 100$, $N_\omega = 100$, $\Delta z = \pi/2$, $n_1^2 = 1.0$. AKSFig3.eps.

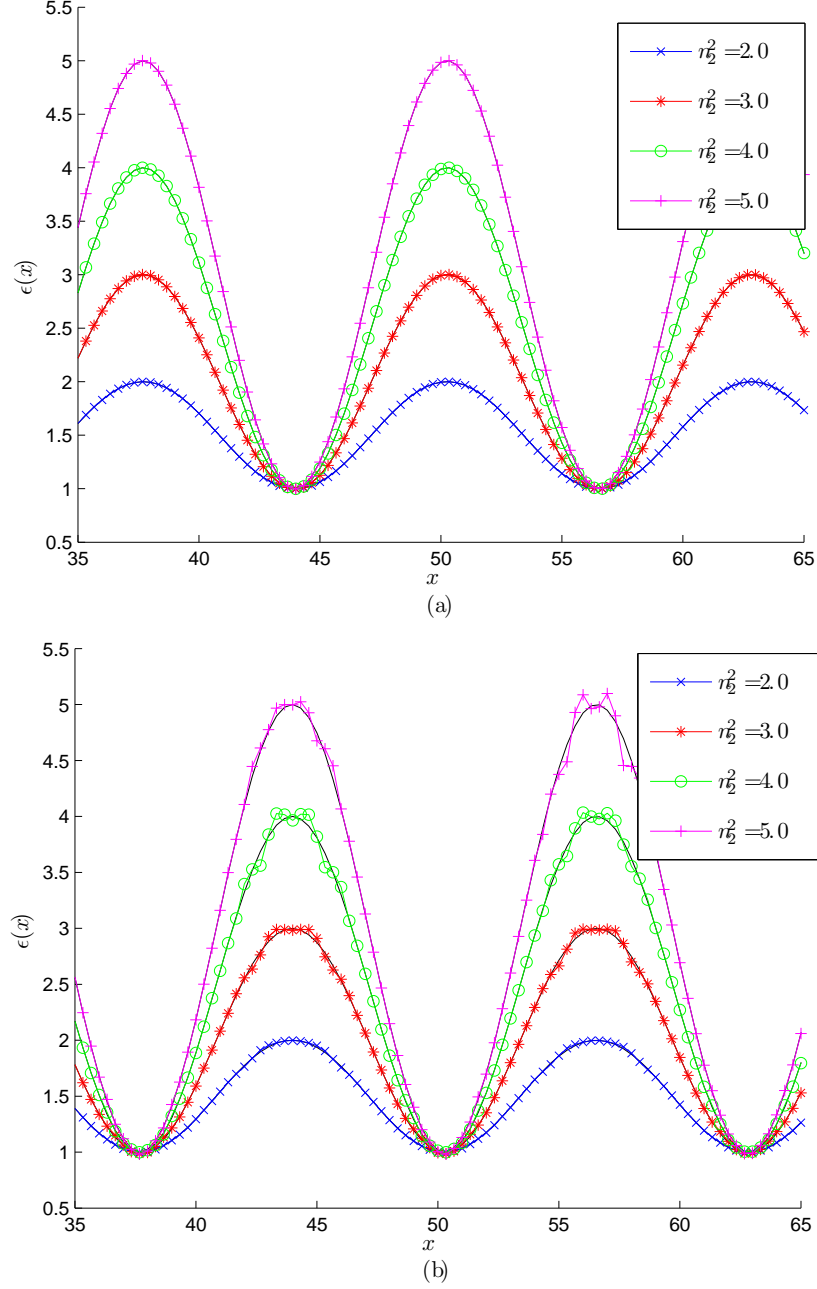


Fig. 4. Reconstruction of the first layer, (a), and the second layer, (b), for different choices of n_2 . Other parameters: $M = 300$, $L = 100$, $\omega \in [9, 19]$, $N_\omega = 100$, $\Delta z = \pi/2$, $n_1^2 = 1.0$. The solid black lines represent the exact permittivity. AKSFig4.eps.

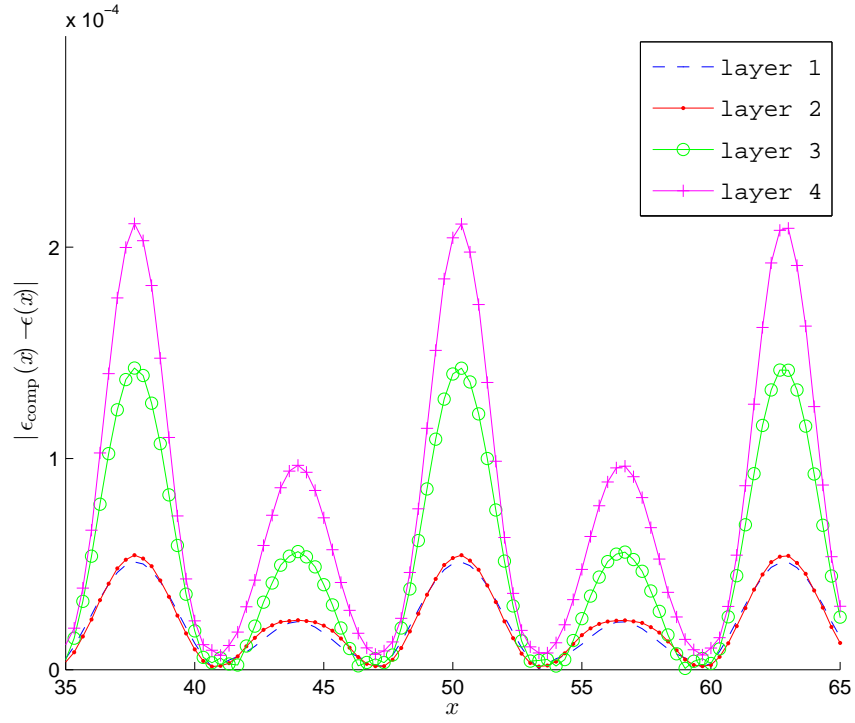


Fig. 5. The error in each layer, given as $|\epsilon_{\text{comp}} - \epsilon|$. Parameters: $M = 300$, $L = 100$, $\omega \in [9, 19]$, $N_\omega = 100$, $\Delta z = \pi/2$, $n_1^2 = 1.0$, $n_2^2 = 1.05$. AKSFig5.eps.

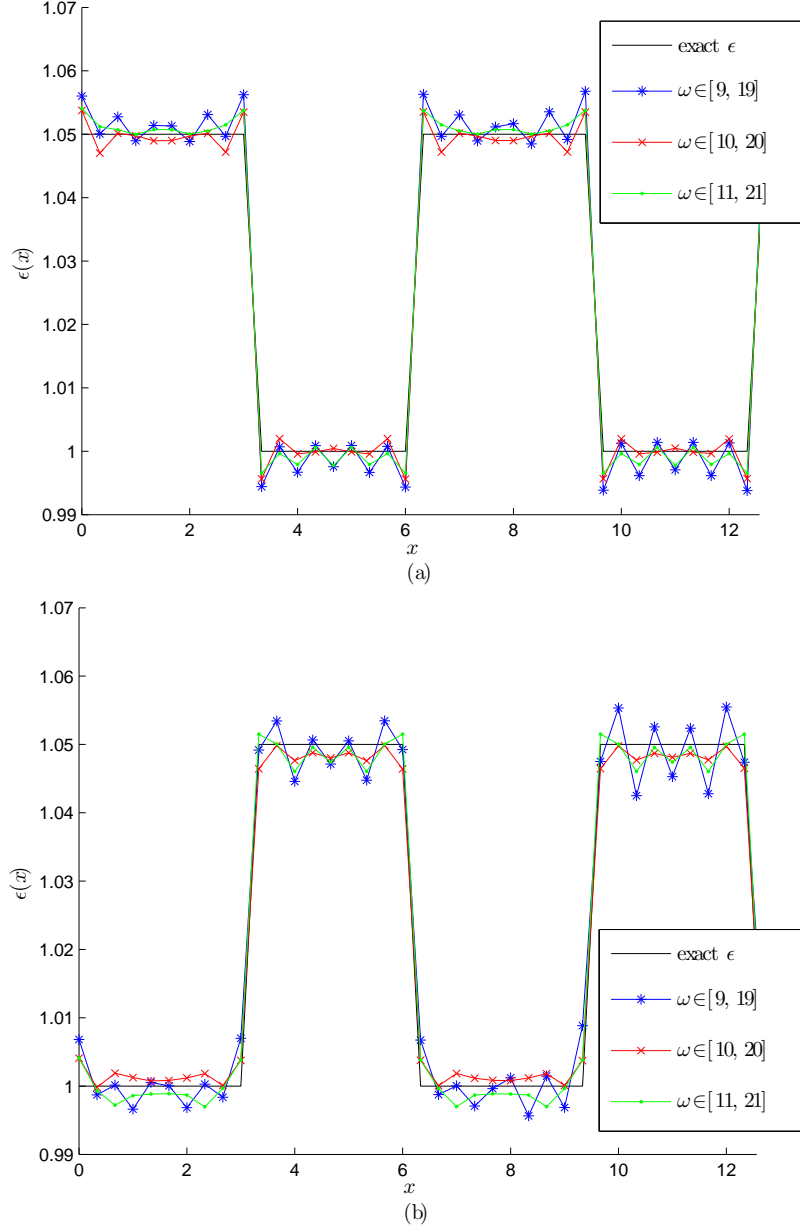


Fig. 6. Reconstruction of the square function for the first layer, (a), and for the second layer, (b). The computations were done for different ω_1 and ω_2 , but with constant bandwidth. Other parameters: $M = 300$, $L = 100$, $N_\omega = 100$, $\Delta z = \pi/2$, $n_1^2 = 1.0$, $n_2^2 = 1.05$. AKSFig6.eps.